Short communication

The effects of upper airway tissue motion on airflow dynamics

Yongling Zhao [a], Joel Raco [b], Agisilaos Kourmatzis [a], Sammy Diasinos [b],
Hak-Kim Chan [c], Runyu Yang [d], Shaokoon Cheng [b,*]

[a] *School of Aerospace, Mechanical and Mechatronic Engineering, The University of Sydney, NSW 2006*
[b] *School of Engineering, Macquarie University, NSW 2109*
[c] *Advanced Drug Delivery Group, School of Pharmacy, The University of Sydney, NSW 2006*
[d] *School of Materials Science and Engineering, UNSW Sydney, NSW 2052*

ABSTRACT

The human upper airway is not only geometrically complex, but it can also deform dynamically as a result of active muscle contraction and motility during respiration. How the active transformation of the airway geometry affects airflow dynamics during respiration is not well understood despite the importance of this knowledge towards improving current understanding of particle transport and deposition. In this study, particle image velocimetry (PIV) measurements of the fluid dynamics are presented in a physiologically realistic human upper airway replica for i) the undeformed case and ii) the case where realistic soft tissue motion during breathing is emulated. Results from this study show that extrathoracic wall motion alters the flow field significantly such that the fluid dynamics is distinctly different from the undeformed airway. Distinctive flow field patterns in the physiologically realistic airway include i) fluid recirculation at the back of the tongue and cranial to the tip of the epiglottis during mid-inspiration, ii) horizontal and posteriorly directed flow at the back of tongue at the peak of inspiration and iii) concentrated flow directed towards the root of tongue near to the end of inspiration. These findings suggest that the active deformation of the human upper airway can potentially influence particle transport by increasing deposition at the back of the tongue and therefore, highlights the importance of considering extrathoracic wall motion in future airway flow studies.

1. Introduction

The interactions between soft tissue movement and biofluid can potentially result in complex flow dynamics as demonstrated in the blood (Ku, 1997; Morshed et al., 2014) and cerebrospinal fluid flow transport (Cheng et al., 2014b; Cheng et al., 2007). The effects of upper airway tissue motion on airflow dynamics are less well understood despite its importance for not only improving knowledge on the transport and deposition of inhaled drugs and pollutants, but also enhancing understanding of

Corresponding author at: Shaokoon Cheng, shaokoon.cheng@mq.edu.au, Macquarie University.

respiratory diseases such as sleep apnea (Bradley and Floras, 2003; Kourmatzis et al., 2018; Zheng et al., 2017).

The extrathoracic airway has been commonly modelled as a passive structure even though measurements of upper airway tissue motility using novel MRI techniques (Cheng et al., 2014a; Cheng et al., 2010) have demonstrated that the pharynx can deform dynamically during respiration. In fact, during inspiration, contraction of the tongue muscle can effectively dilate the airway at the level of the epiglottis, and this is very different from how a passive airway model would respond. In addition, the pharynx is formed by soft tissues and muscles with complex mechanical properties (Brown et al., 2015) and deformation of the upper airway takes place at specific locations. Hence, representing the tissue mass that surrounds the airway by a membrane is insufficient, and airway wall movement needs to be controlled and simulated to emulate realistic upper airway physiology. There are three general patterns of upper airway deformation in humans (Cheng et al., 2010), and the effects of this complex airway motion have not been considered in existing studies of airway flow dynamics.

Particle imaging velocimetry (PIV) is a useful tool that has been widely adopted by the fluid mechanics community (Groß et al., 2008; Zhao et al., 2019) to investigate complex local and global flow structures in the airways ((Chung and Kim, 2008; Doorly et al., 2008; Hopkins et al., 2000; Kelly et al., 2000; Kim and Chung, 2004; Spence et al., 2012; Spence et al., 2011). Previous experimental studies have provided insights into fluid dynamics in upper airways under various physiologically realistic conditions which are critical to validate the accuracy of computational models. In this study, lateral deformation of the airway at the level of the soft palate (Cheng et al., 2010; Schwab et al., 2003) will be physically simulated to provide the first insights on the effects of upper airway muscle motility on airflow dynamics at the level of epiglottis given that this is the narrowest section of the pharynx.

2. Methods

2.1 Fabrication of the upper airway model

A three-dimensional model of the upper airway was reconstructed using a set of MRI images and 3D Slicer (www.slicer.org, (Fedorov et al., 2012)). A voxel size of 0.25 mm was used to form an image stack with dimensions that consist of 276 voxels by 448 voxels by 468 voxels. The reconstructed 3D upper airway model was then exported to Rhinoceros (www.rhino3d.com), and moulds were designed using the surfaces of the upper airway and fabricated using a 3D printer. The airway model with a wall thickness of ~ 3 mm was then manufactured using optically accessible silicone and inverse casting.

2.2 PIV setup

The experimental setup (Fig 1a) consisted of i) an upper airway replica, ii) a glass tank (200 mm × 350 mm × 100 mm), iii) a pump system actuated by a stepper motor and lead screw, iv) a reservoir that contains the working fluid and 20 μm polyamide seeding particles (PSP, from Dantec Dynamics), v) a mechanical pincher that synchronises with the pump, vi) a pco. camera (spatial resolution - 1600 pixel × 1200 pixel) and vii) a double-pulse Nd:YAG laser (EverGreen). A mixture of water (56%) and glycerine (44%) was used to match the refractive index of the airway model, and optical accessibility was validated using a grid test (See Fig 1d).

The camera was positioned at ~ 200 mm away from the laser sheet. The field of view (FOV) was 50 mm × 37.5 mm and was situated at a location beneath the deformation region of the airway replica to investigate the flow field around the epiglottis. A density of 5~10 particles per interrogation window was achieved in the measurements. The recording of particle images employed a double-frame mode, and the imaging frequency was 5 Hz due to the low flow velocity. Digital cross-correlation was used in image processing to determine the displacement of particles, in which a triple-pass cross-correlation with interrogation windows starting from 128 pixels × 128 pixels with 50% overlap was adopted. The ILA GmbH software is utilized for image processing.

2.3 Measurement protocol

Deformation of the upper airway replica was synchronised with the fluid flow, and both were controlled using an in-house synchronising system, which was calibrated and verified before performing the PIV measurements. The magnitude of the flow rate at the peak of inspiration and expiration was 3.70 litre per minute, and this matches with a Reynolds number (*Re:* 1060*)* that represents 5 litres per minute of airflow in the actual human pharynx. The flow rate used is physiologically realistic, and the low flow rate was chosen as a first study to ensure that deformation of the airway did not result in any passive collapse of the airway downstream. A Womersley number of 3.43 was used in the experiments to match a slow breathing condition. The magnitude of airway deformation was determined by the distance between the pincher arms which was ~ 10 cm at time points I and III and 30 cm when the airway was not deformed. Images were collected at time points I, II and III, and they correspond to 33%, 50% and 33% of airway deformation respectively. It is noteworthy that these levels of deformation have been observed in previous MRI experiments (Cheng et al., 2014). The ensemble averaging of the flow field was achieved over 20 complete respiratory cycles for each time point. The imaging sample size (n = 20) was determined from preliminary studies,

which showed that increasing the sample size did not result in any noticeable changes in the flow field at the three imaging time points.

3. Results and Discussion

3.1 Flow field at time point I

There are distinctive differences in flow fields between the models with and without deformation at three specific airway regions (see velocity vectors shown in regions A, B and C in Figure 3). Region A consists of a recirculation zone, and an unsteady flow regime as the airway deforms, and this is in stark contrast with the flow field in the undeformed airway where flow in the same region is clearly homogeneous. Also, while there is a weak swirling flow in region B as the airway deforms, the fluid flow is laminar and directed mainly downward in region B in the undeformed airway. The effects of airway deformation are less significant downstream of the airway (Region C) where the flow fields are similar in both models.

3.2 Flow field at time point II

The flow field in the deformed airway at time point II (Fig. 4) is significantly different from the undeformed airway upstream (region A) and downstream (region B) of the epiglottis. As the airway deformed, horizontal and posteriorly directed flow was induced at the back of the tongue (see region A), and such a flow pattern led to the formation of a large vortex at the same region during time point III (Fig. 5). Flow in the deformed airway was more homogeneous across the airway section than the undeformed airway downstream from the epiglottis (see region B). In the undeformed airway, a high-speed jet flow adjacent to the anterior airway wall can be observed, and this is essentially an 'extension' of the upstream fluid flow exiting the epiglottis. Adjacent to this high-speed region is a distinctive low velocity "dead-region" (see Region B). As the airway deformed, the streamwise velocity increased ("enhanced-region"), and this may advantageously transport fine particles that have not been deposited onto the tongue, to the lower airways.

3.3 Flow field at time point III

Towards the end of inspiration, the horizontal and posteriorly directed flow which occurred at time point II led to the development of a vortex (see Region A, Figure 5) which was not observed in the undeformed airway. The vortex spanned a considerably large section of the airway that represented approximately one-third of the airway width. Contrary to the undeformed airway, the flow was also more prominent along the boundary of the epiglottis in the deformed airway model (See Region B). For example, in the deformed airway model, the concentration of flow vectors directed towards the

root of the tongue can be observed (see Region C). Particles deposited in this region are more likely to be swallowed. Similar to the flow field downstream to the epiglottis in time point II, there was also a "dead-region" and "enhanced-region".

4. Implications and Conclusion

To the best of the author's knowledge, this is the first experimental study that demonstrates differences in airflow dynamics between an actively deforming and undeformed upper airway during respiration. Results from this study show that the lateral deformation of the upper airway at the level of the soft palate will potentially change the flow fields throughout the respiratory cycle. Key changes observed include a swirling flow at the back of the tongue (time point I), a horizontal flow directed towards the back of the tongue (time point II) and establishment of a dominant vortex upstream of the epiglottis (time point III). These flow patterns which are absent in the undeformed airway are likely to increase particle deposition on the tongue and may present a different particle deposition profile compared to a rigid upper airway, which merits further investigation. It is interesting to note that the flow field at time points I and III is distinctly different despite having the same flow rate. The difference is related to the differences in residual flow and dynamic airway deformation where the airway is collapsing at time point I but decompressing at time point III. Future studies using higher flow rates and simulating other more complex upper airway deformation patterns and flow profile are warranted to enhance our current understanding of physiologically realistic airway flow mechanics.

Acknowledgements

Funding for this publication was made possible, in part, by the Australian Research Council through grant DP190101237 and the Food & Drug Administration (United States) through grant 1U01FD006525 - 01. Views expressed do not necessarily reflect the official policies of the Department of Health and Human Services; nor does any mention of trade names, commercial practices, or organization imply endorsement by the United States Government.

References

Bradley, T.D., Floras, J.S., 2003. Sleep Apnea and Heart Failure. Circulation 107, 1671-1678.

Brown, E.C., Cheng, S., McKenzie, D.K., Butler, J.E., Gandevia, S.C., Bilston, L.E., 2015. Tongue Stiffness is Lower in Patients with Obstructive Sleep Apnea during Wakefulness Compared with Matched Control Subjects. Sleep 38, 537-544.

Cheng, S., Brown, E.C., Hatt, A., Butler, J.E., Gandevia, S.C., Bilston, L.E., 2014a. Healthy humans with a narrow upper airway maintain patency during quiet breathing by dilating the airway during inspiration. The Journal of Physiology 592, 4763-4774.

Cheng, S., Butler, J.E., Gandevia, S.C., Bilston, L.E., 2010. Movement of the human upper airway during inspiration with and without inspiratory resistive loading. Journal of Applied Physiology 110, 69-75.

Cheng, S., Fletcher, D., Hemley, S., Stoodley, M., Bilston, L., 2014b. Effects of fluid-structure interaction in a three dimensional model of the spinal subarachnoid space. Journal of Biomechanics 47, 2826-2830.

Cheng, S., Jacobson, E., Bilston, L.E., 2007. Models of the pulsatile hydrodynamics of cerebrospinal fluid flow in the normal and abnormal intracranial system. Computer Methods in Biomechanics and Biomedical Engineering 10, 151-157.

Chung, S.K., Kim, S.K., 2008. Digital particle image velocimetry studies of nasal airflow. Respiratory Physiology & Neurobiology 163, 111-120.

Doorly, D., Taylor, D.J., Franke, P., Schroter, R.C., 2008. Experimental investigation of nasal airflow. Proceedings of the Institution of Mechanical Engineers, Part H: Journal of Engineering in Medicine 222, 439-453.

Fedorov, A., Beichel, R., Kalpathy-Cramer, J., Finet, J., Fillion-Robin, J.-C., Pujol, S., Bauer, C., Jennings, D., Fennessy, F., Sonka, M., Buatti, J., Aylward, S., Miller, J.V., Pieper, S., Kikinis, R., 2012. 3D Slicer as an image computing platform for the Quantitative Imaging Network. Magn Reson Imaging 30, 1323-1341.

Groß, S., Schröder, W., Klaas, M., 2008. Time-Resolved PIV Measurements of Vortical Structures in the Upper Human Airways, Particle Image Velocimetry: New Developments and Recent Applications. Springer Berlin Heidelberg, Berlin, Heidelberg, pp. 35-53.

Hopkins, L.M., Kelly, J.T., Wexler, A.S., Prasad, A.K., 2000. Particle image velocimetry measurements in complex geometries. Exp. Fluids 29, 91-95.

Kelly, J.T., Prasad, A.K., Wexler, A.S., 2000. Detailed flow patterns in the nasal cavity. Journal of Applied Physiology 89, 323-337.

Kim, S.K., Chung, S.K., 2004. An investigation on airflow in disordered nasal cavity and its corrected models by tomographic PIV. Measurement Science and Technology 15, 1090-1096.

Kourmatzis, A., Cheng, S., Chan, H.K., 2018. Airway geometry, airway flow, and particle measurement methods: implications on pulmonary drug delivery. Expert Opinion on Drug Delivery 15, 271-282.

Ku, D.N., 1997. Blood Flow in Arteries. Annu. Rev. Fluid Mech. 29, 399-434.

Morshed, K.N., Bark Jr, D., Forleo, M., Dasi, L.P., 2014. Theory to Predict Shear Stress on Cells in Turbulent Blood Flow. PLOS ONE 9, e105357.

Schwab, R.i.J., Pasirstein, M.J., Pierson, R.E., Mackley, A., Hachadoorian, R., Arens, R., Maislin, G., Pack, A.I., 2003. Identification of upper airway anatomic risk factors for obstructive sleep apnea with volumetric magnetic resonance imaging. American journal of respiratory and critical care medicine, 522-530.

Spence, C.J.T., Buchmann, N.A., Jermy, M.C., 2012. Unsteady flow in the nasal cavity with high flow therapy measured by stereoscopic PIV. Exp. Fluids 52, 569-579.

Spence, C.J.T., Buchmann, N.A., Jermy, M.C., Moore, S.M., 2011. Stereoscopic PIV measurements of flow in the nasal cavity with high flow therapy. Exp. Fluids 50, 1005-1017.

Zhao, Y., Lei, C., Patterson, J.C., 2019. PIV measurements of the K-type transition in natural convection boundary layers. Experimental Thermal and Fluid Science, 62-75.

Zheng, Z., Liu, H., Xu, Q., Wu, W., Du, L., Chen, H., Zhang, Y., Liu, D., 2017. Computational fluid dynamics simulation of the upper airway response to large incisor retraction in adult class I bimaxillary protrusion patients. Scientific Reports 7, 45706.

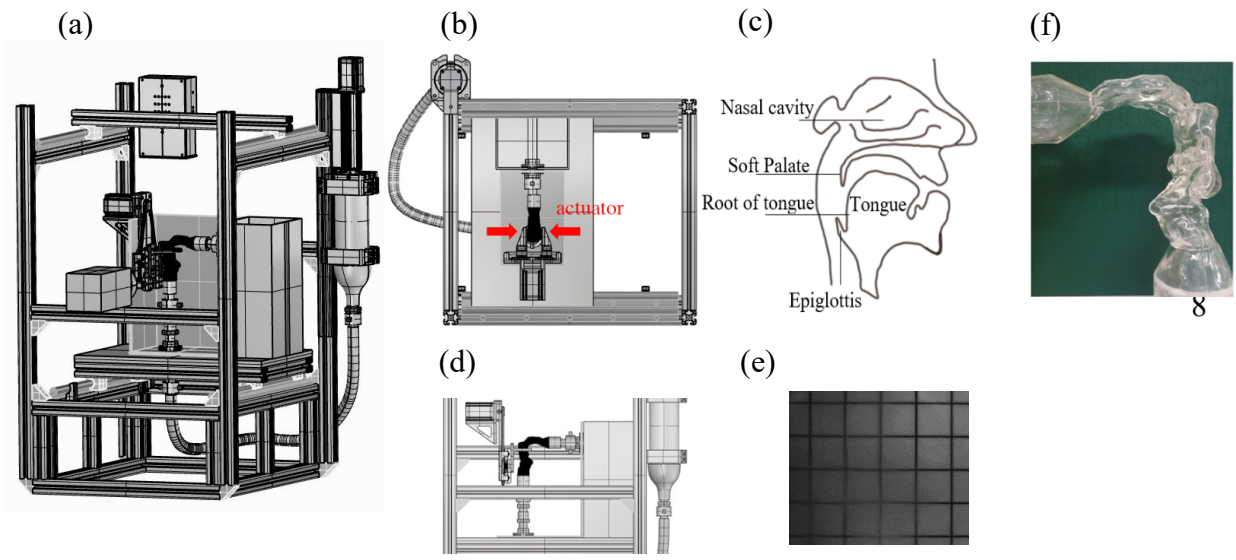

Fig. 1 (a) Experimental setup, (b) top-view showing how the airway was deformed, (c) anatomical landmarks of the upper airway, (d) side-view of the experimental setup showing the location of deformation, (e) grid test – image was taken with airway replica in front of the grid lines to demonstrate that there were no image distortion and (f) actual airway replica.

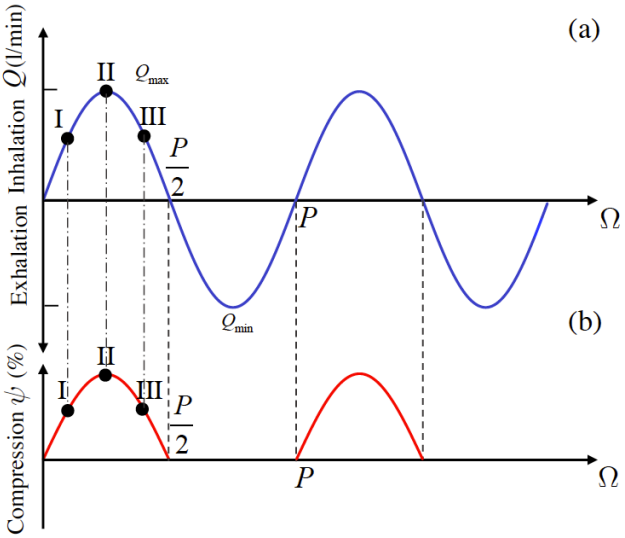

Fig. 2. Panel shows the a) Respiratory flow profile and b) profile of airway lateral deformation at the soft palate. The black coloured dots (I,II and III) represent the time points where the images were taken and the period of the respiratory cycle respectively. The compression $\boldsymbol{\psi}$ is 33%, 50% and 33% for time points I, II and III respectively.

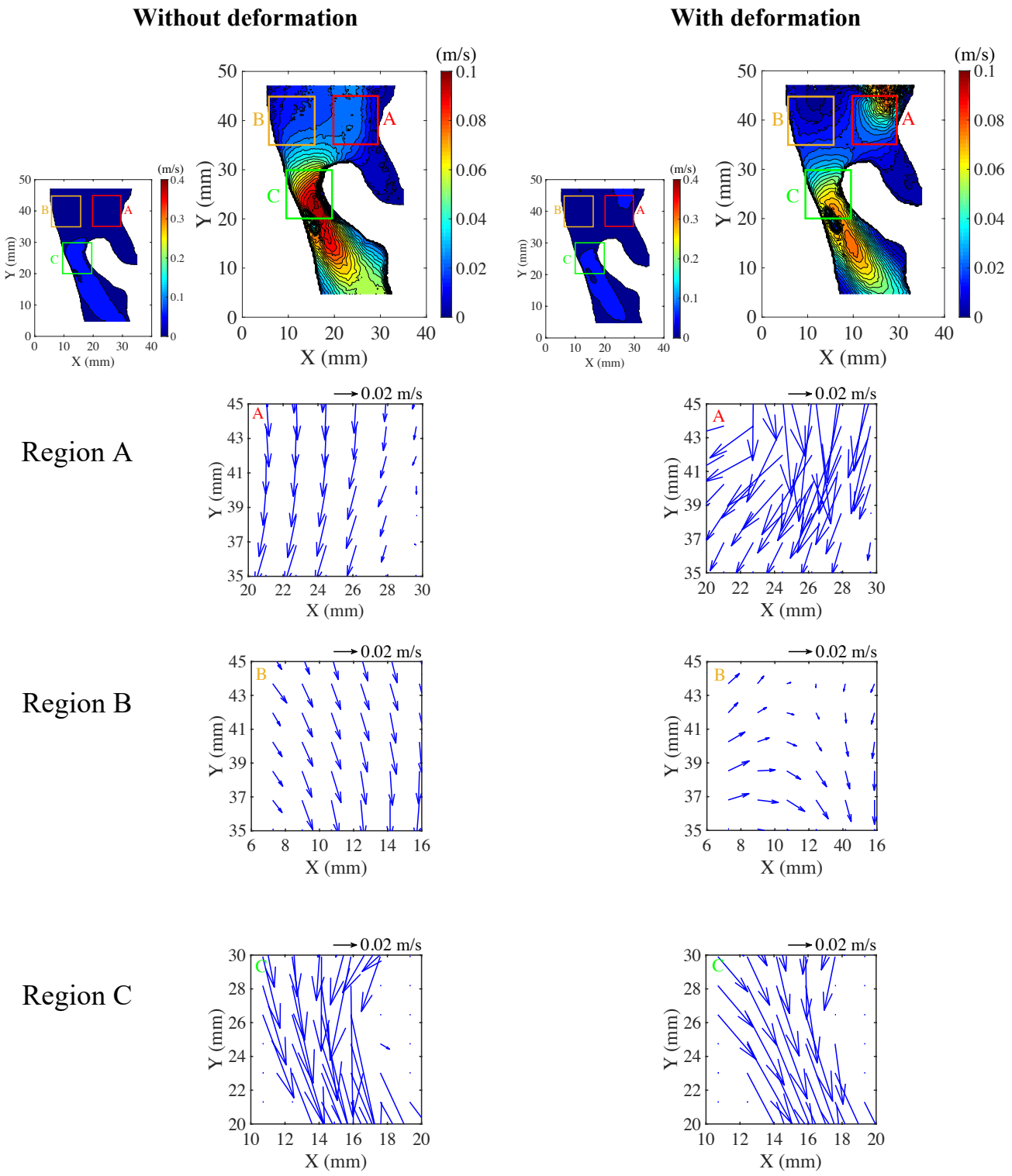

Fig. 3 Flow field at time point 1. The panel shows detailed flow field patterns at three regions (A, B and C) in the deformed and undeformed upper airway. Note that filled contour plots show the magnitude of velocities and vector fields are produced using the same data.

1

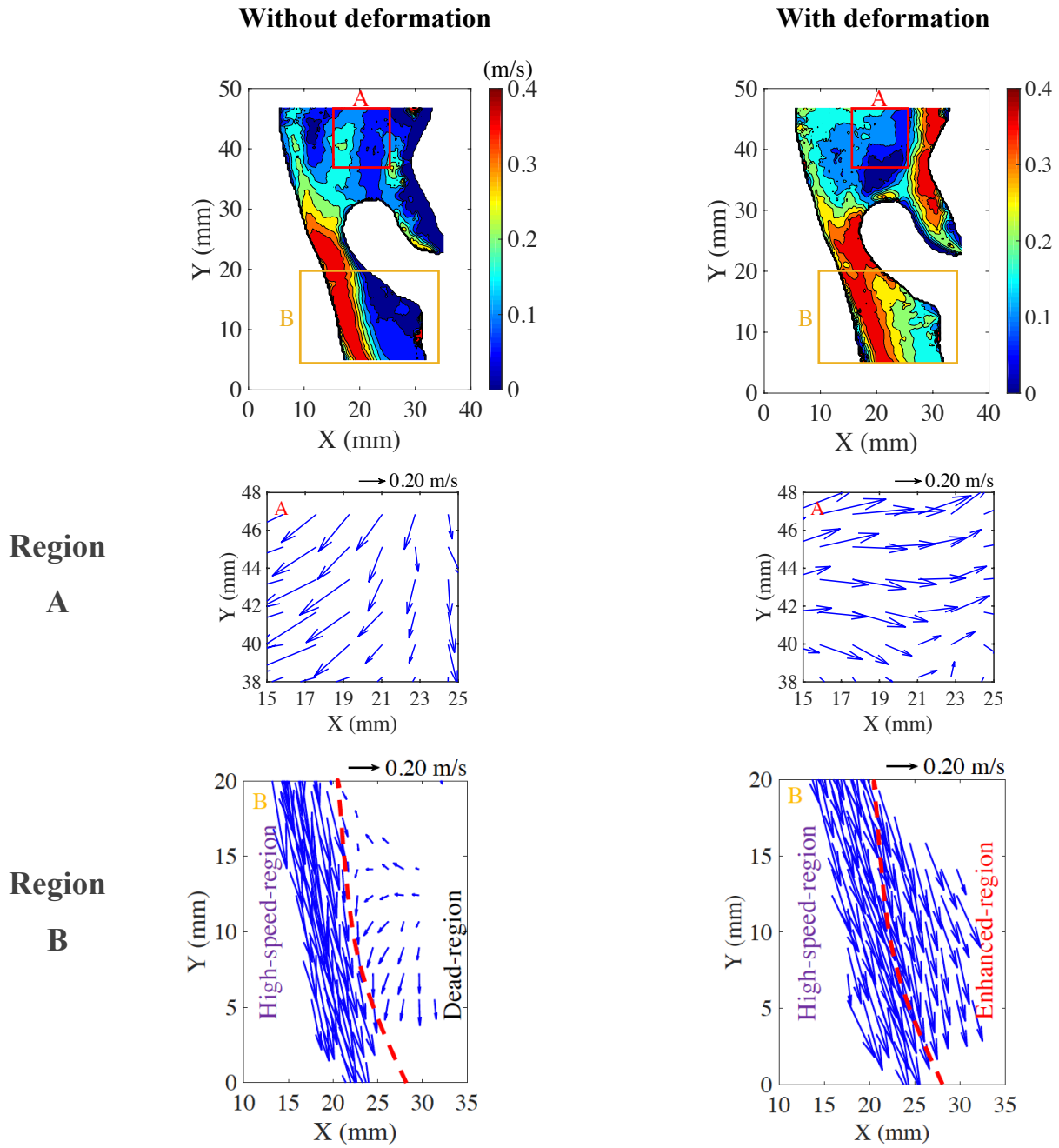

Fig. 4 Flowfield at time point II.

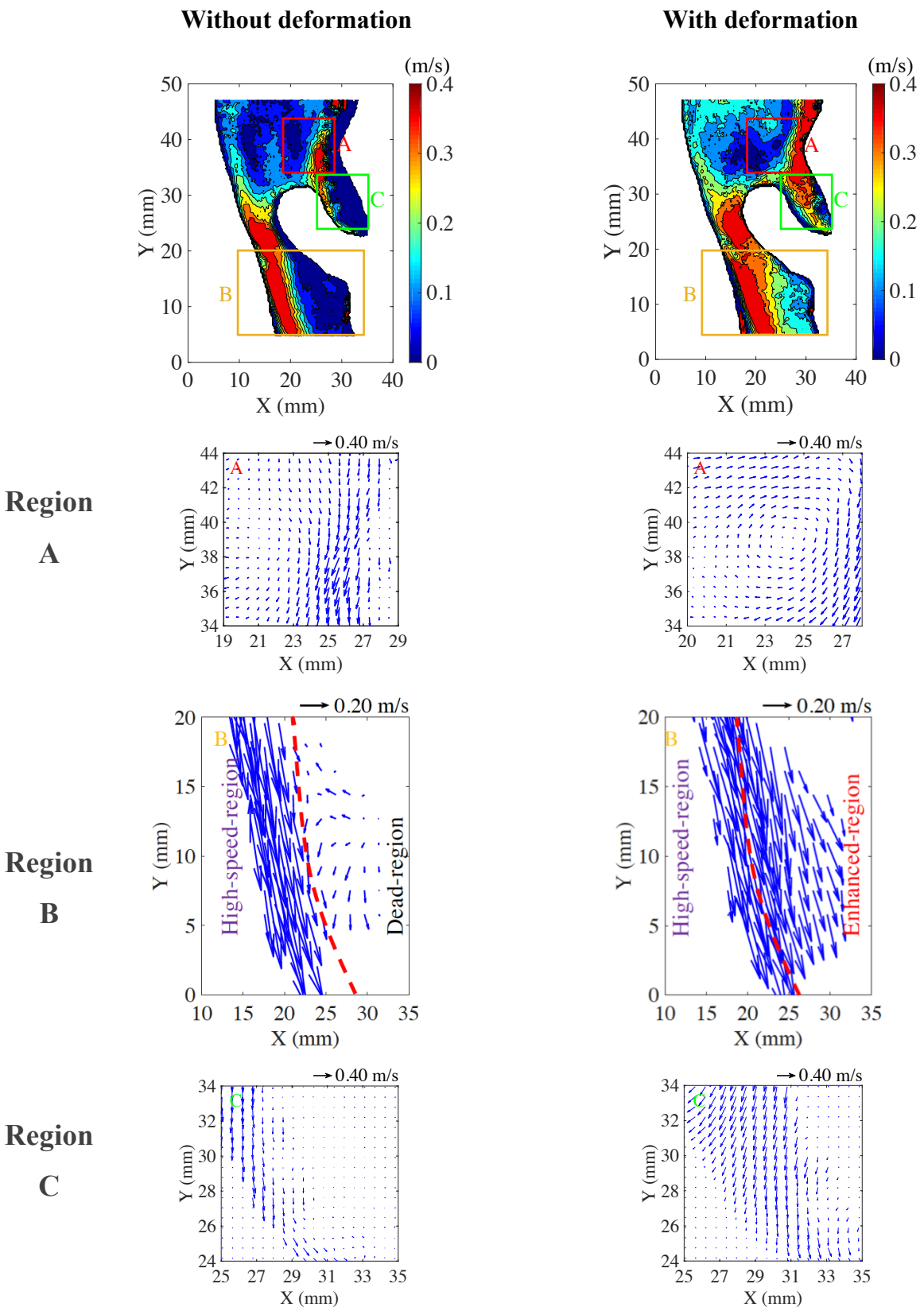

Fig. 5 Flowfield at time point III.

1